remote sensing

MDPI

Article

Reflectance–Elevation Relationships and Their Seasonal Patterns over Twelve Glaciers in Western China Based on Landsat 8 Data

Xinwu Li [1], Wenjin Wu [1,*], Baiqing Xu [2], Siyang Yin [1], Ruifang Yang [3] and Shu Cheng [4]

[1] Institute of Remote Sensing and Digital Earth, Chinese Academy of Sciences, 100094 Beijing, China; lixw@radi.ac.cn (X.L.); yinsy@radi.ac.cn (S.Y.)
[2] Institute of Tibetan Plateau Research, Chinese Academy of Sciences, 100101 Beijing, China; baiqing@itpcas.ac.cn
[3] School of Civil Engineering, Beijing Jiaotong University, 100044 Beijing, China; 14121165@bjtu.edu.cn
[4] School of Geosciences and Info-Physics, Central South University, 410083 Changsha, China; cheng_shu@163.com
* Correspondence: wenjin.wu.happy@gmail.com; Tel.: +86-10-8217-8109

Academic Editors: Frank Paul, Kate Briggs, Robert McNabb, Christopher Nuth, Jan Wuite, Xiaofeng Li and Prasad S. Thenkabail
Received: 15 December 2016; Accepted: 20 February 2017; Published: 23 February 2017

Abstract: Albedo/reflectance is of great importance for glaciers' mass balance and energy budget. Elevation could be a major factor of influence for glacier reflectance, and therefore when studying glacier reflectance, the altitude ranges should be considered. However, due to the limitations of traditional earth observation systems, conventional analyses usually consider the spatial and temporal patterns of the reflectance average, which is severely restricted. The launch of Landsat-8 gives us the opportunity to study the seasonal glacier reflectance–elevation relationship. We have obtained the monthly near-nadir reflectance per 100 m for twelve glaciers in western China based on 372 scenes of Landsat 8 images acquired from April 2013 to December 2015. Variations of monthly broadband reflectance, reflectance–elevation relationships and reflectance gradients are analyzed and discussed. The results show that the linear trend of the reflectance–elevation relationship (when the altitude is less than 6100 m) is very significant; elevation has greater influence than location on seasonal reflectance variations; and the level of glacier reflectance gradient may relate with its climate. This may be the first work that has used remote-sensing data to analyze seasonal glacier reflectance–elevation patterns.

Keywords: glacier monitoring; Landsat-8; glacier reflectance–elevation relationship

1. Introduction

Reflectance is one of the most important properties of glaciers, controlling their surface energy and reflecting the distribution of snow and ice on their surfaces. Typically, solar radiation provides about 75 percent or more of the melt energy for glaciers in summer [1]. Decreasing reflectance is a vital reason for glacier ablation, and, as a feedback, melting can further decrease reflectance and help accelerate deglaciation [2,3]. Seasonal or monthly glacier reflectance variation is an indicator that reflects the timing of precipitation events, which is vital information for water equivalent researches [1]. Glacier reflectance–elevation relationships can reveal the spatial distribution of the snow cover, and assist to study the glacier mass balance and energy budget. Glacier reflectance/albedo has been obtained using both ground-based measurements and remote-sensing technologies [4–10]. The advantages and shortcomings of these two data acquisition methods have been compared [11]. MODIS and Landsat are two favored remote-sensing datasets used to derive glacier albedo or reflectance. MODIS

has the 16-day combined 500 m/1000 m/5600 m resolution albedo products MCD43A, MCD43B, and MCD43C, inverted with multi-data, multi-angular, cloud-free and atmospherically corrected images [12]. Because of its spatial resolution and covering capacity, the product is usually used to analyze albedo or reflectance variations over a large area. Landsat has provided multispectral data with the 30 m resolution and a 16-day repeat cycle since the 1970s. It can only measure the near-nadir reflectance, and so cannot be used to derive absolute glacier albedo directly. However, this is not a problem when analyzing the monthly or seasonal elevation-related variation trend of reflectance on glaciers. Another major problem when using the dataset is cloud cover, which often leads to discontinuous usable images for a given location. Fortunately, the situation is much improved since the launch of Landsat 8. Compared with Landsat 7, approximately 60% more Landsat 8 scenes are acquired per day, with near-global seasonal coverage [13,14].

Factors that can alter the glacier albedo/reflectance such as snowfall, glacier melting, penitents (snow formations found at high altitudes [15]), surface dust, snow algae, and impurities in ice have been analyzed in depth [2,16–20]. Elevation could be a major factor of reflectance over clean glaciers, because temperature drops with the increasing altitude and melting decreases. Therefore, when analyzing the reflectance patterns for glaciers, the altitude range should be considered. Studying the reflectance–elevation relationship is thus an interesting topic. However, few studies [16,20,21] have addressed the observed temporal variations of glacier reflectance–elevation relationships. These studies usually focus on a particular glacier with a small altitude range, and the temporal series are also discontinuous. The pattern of reflectance–elevation relationship is hard to reveal. This is probably because of the limitations of the data source since the field observation sites are scattered, resolution of the MODIS dataset is inadequate to generate smooth reflectance–elevation signatures, and the temporal series of Landsat data is usually fragmentary. As mentioned above, research on monthly or at least seasonal reflectance–elevation relationships over glacial areas is now realizable thanks to the free Landsat 8 dataset [22], and we present an example of such research here. Monthly broadband near-NADIR reflectance per 100 m was obtained for twelve glaciers in western China based on 372 scenes of Landsat 8 images acquired from April 2013 to December 2015. Variations of monthly reflectance–elevation relationships and reflectance gradients are analyzed and discussed.

2. Datasets and Methods

The study area is located in western China. Twelve glaciers in the Qilian, Himalaya, Danggula, Pamir and Karakorum mountains were chosen considering the available data, glacier elevation, climate, and geographical distribution. The chosen glaciers span 3100-m elevation range and basically cover all the typical regions in western China. Note that some regions have more cloud cover which limits the data acquisition, and therefore the selection may have a tendency to choose glaciers in areas with good year-round weather conditions. Information on these glaciers is shown in Table 1, and their locations are labeled in Figure 1. Most of them are summer accumulation type glaciers which are mainly influenced by the summer monsoon, and receive most annual precipitation in summer [23]. Their latitudes range from 28°N to 40°N and are mainly in the temperate zone and mid- latitudes. Summer accumulation type glaciers are especially vulnerable to global warming [24], so analysis of these glaciers is of particular interest. The altitudes of the selected glaciers extend from 4200 to 7300 m, with (12) Qiyi the lowest, ranging from 4200 m to 5200 m, and (5) Naimona'nyi the highest, ranging from 5500 to 7300 m. We can observe from Table 1 that two pairs of glaciers ((8) Hariqin and (3) Muztagata; and (10) Meikuang and (1) Muji) have similar altitude extents, but are from different mountains. Three pairs of glaciers ((2) Kangxiwar and (3) Muztagata; (8) Hariqin and (7) Xiaodongkemadi; and (9) Yuzhu Peak and (10) Meikuang) are adjacent to each other, providing good comparability in the analysis. As a benefit from this comparability, we constitute two glacier groups considering their locations and altitudes for further comparison. Group (A) comprises: (1) Muji; (9) Yuzhu Peak; and (10) Meikuang. (1) Muji and (10) Meikuang have identical elevation extents, and (9) Yuzhu Peak and (10) Meikuang are contiguous. Group (B) comprises: (2) Kangxiwar; (3) Muztagata; (8) Hariqin;

and (7) Xiaodongkemadi. (3) Muztagata and (8) Hariqin have the same elevation extent and are, respectively, adjacent to (2) Kangxiwar and (7) Xiaodongkemadi. We think the analysis of these two groups of glaciers can help us understand the dominant factors of glacier reflectance, because the environmental factors such as temperature and precipitation mainly vary with altitudes and locations.

Table 1. Information on the twelve selected glaciers in western China. The last column presents the actual altitude extent used to obtain the results.

No.	Glacier Name	Mountain	Latitude (°N)	Longitude (°E)	Mid-Point Elevation (m)	Altitude Extent (m)	Altitude Extent after Processing (m)
1	Muji	Pamir	39.187	73.742	5100	4700–5600	4700–5500
2	Kangxiwar	Pamir	38.411	75.323	5100	4900–5400	4900–5200
3	Muztagata	Pamir	38.238	75.061	5600	5200–6000	5200–5900
4	Kunjirap	Karakorum	36.818	75.453	5200	4900–5600	4900–5400
5	Naimona'nyi	Himalayas	30.457	81.326	6400	5500–7300	5500–7200
6	Langariding	Himalayas	28.348	90.066	6000	5800–6300	5800–6100
7	Xiaodongkemadi	Danggula	33.069	92.073	5600	5200–6100	5300–5900
8	Hariqin	Danggula	33.140	92.093	5600	5200–6000	5200–5800
9	Yuzhu Peak	Kunlun	35.645	94.227	5600	5100–6200	5100–5800
10	Meikuang	Kunlun	35.673	94.186	5100	4700–5600	4700–5500
11	Qiumianleiketage	Kunlun	36.696	90.729	5500	5100–5900	5100–5600
12	Qiyi	Qilian	39.241	97.758	4700	4200–5200	4200–5100

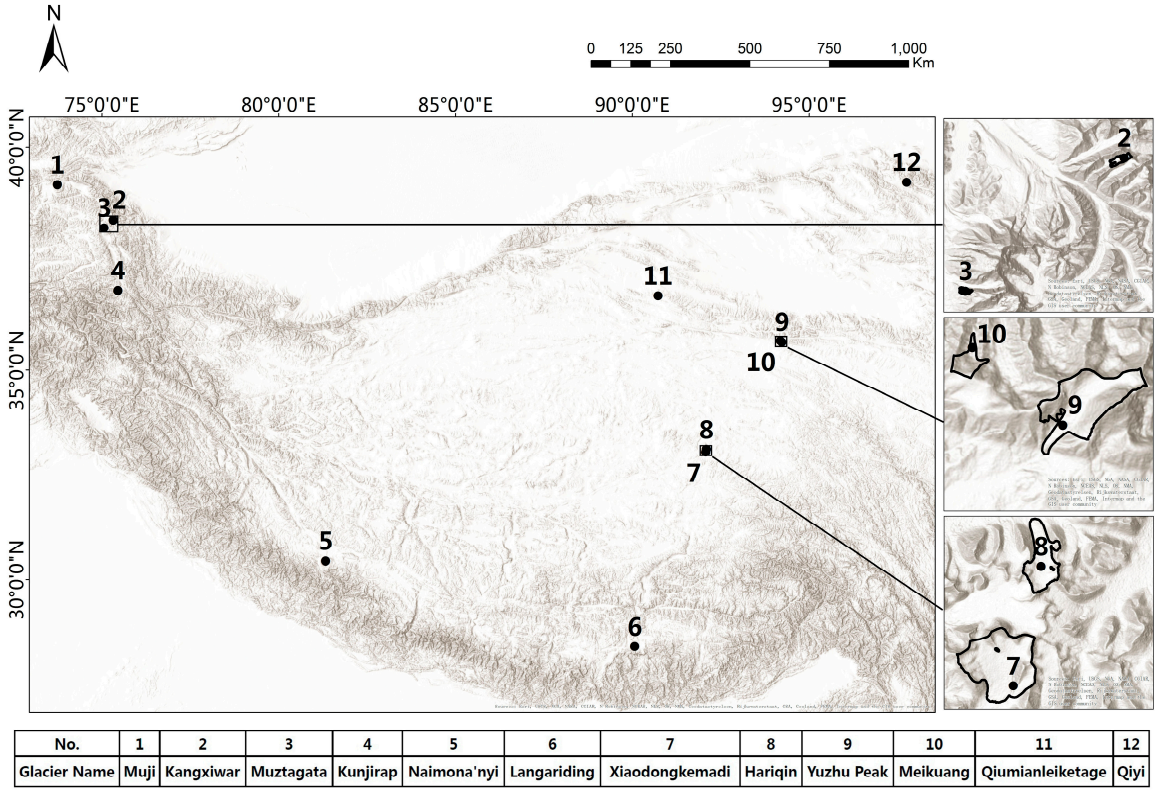

No.	1	2	3	4	5	6	7	8	9	10	11	12
Glacier Name	Muji	Kangxiwar	Muztagata	Kunjirap	Naimona'nyi	Langariding	Xiaodongkemadi	Hariqin	Yuzhu Peak	Meikuang	Qiumianleiketage	Qiyi

Figure 1. Locations of the twelve selected glaciers displayed on a hill shade of a DEM © 1995–2016 Esri [25].

To obtain the reflectance gradients of these twelve glaciers, we collected all the available Landsat 8 data until the start of this work for the corresponding regions. The vector data of selected glaciers are from the published dataset of the second glacier inventory of China in December 2014 [26]. A total of 372 Landsat 8 images were collected from April 2013 to December 2015. All the images were acquired around local 10:30 a.m. (equivalently 12:30 p.m., China standard time) as a compromise between terrain shadow at low solar elevations and development of cloud cover closer towards noon.

Landsat 8 operates in the visible, near-infrared, short wave infrared, and thermal infrared spectrums, and provides imagery with resolution of 15/30/100 m (panchromatic/multispectral/thermal) of Earth's land surface and polar regions [14]. It regularly acquires 725 scenes per day (Landsat 7 acquires 438 scenes per day). This increases the probability of capturing cloud-free scenes for the global landmass [22]. For all twelve glaciers, almost every month has image acquisition, which provides the possibility for inversion of monthly or seasonal reflectance gradients. A digital elevation model (DEM) is also required. Therefore, we have collected the Advanced Spaceborne Thermal Emission and Reflection Radiometer Global Digital Elevation Model (ASTER GDEM) V002 data [27]. The spatial resolution of this DEM product is about 30 m and the altitude precision is 20 m. The product was published in October 2011 and is a good match for the Landsat 8 data in the spatial resolution. The GDEM product was validated by organizations such as USGS, NASA, and NGA using other DEM products and benchmarks in 2011, and the average elevation error is around 12 m [27]. Considering that we only use the DEM to analyze the variation trend of glacier reflectance for every 100 m, the accuracy is enough for the study.

Figure 2 presents a flowchart of the extraction of monthly broadband near-nadir reflectance–elevation relationship using time series Landsat 8 OLI data, glacier vectors, and ASTER GDEM V002 data of the twelve selected glaciers. The SRTM DEM has not been used due to its earlier acquisition date. Before processing, all the Landsat 8 images obtained are manually checked to ensure adequate data quality, which means the glaciers should not be covered by clouds. The GDEM products are reprojected into the UTM projection (the projection zone of each DEM image is decided by the longitude extent) and resampled using the nearest neighbor interpolating method and 25-pixel triangulation warping [28] to match the Landsat 8 imagery. The calibration method used to obtain reflectance from DN values in units of $Wm^{-2}{\cdot}sr^{-1}{\cdot}\mu m^{-1}$ is provided by USGS [29]. The Quick Atmospheric Correction (QUAC) [30] is applied to implement the atmospheric correction. The QUAC determines atmospheric correction parameters directly from the observed pixel spectra in the scene, with no requirement for ancillary information. It is thus more suitable for batch processing, though it performs a more approximate atmospheric correction than the Fast Line-of-sight Atmospheric Analysis of Hypercubes (FLAASH) [31] and other physics-based methods. Its deviation is generally within 10% of the ground truth reflectance spectra [32]. Finally, we adopt the method proposed in [33] to convert narrow-band reflections to the broadband reflectance. The band indexes are modified to fit the spectral bands of Landsat 8.

$$\alpha_{short} = 0.356\alpha_2 + 0.130\alpha_4 + 0.373\alpha_5 + 0.085\alpha_6 + 0.072\alpha_7 - 0.0018 \quad (1)$$

where α_{short} is the shortwave reflectance and α_i is the spectral reflectance in band i of OLI.

To obtain the reflectance–elevation signatures, glacier vectors are divided into 100 m intervals referring to the altitudes in the GDEM product. Reflectance within each vector partition is averaged to reveal the relationship between reflectance and elevations for each glacier. The Topographic/C-correction tool [34] is adopted to implement the terrain effect which considers the solar elevation angle, solar azimuth angle, and local DEM. Glaciers on slopes inclined away from the sun will result in shadows and affect the reflectance estimation. Therefore, glacier areas in shadows are excluded for each image in the post-processing. Moreover, cloud areas over the glaciers are also excluded before the reflectance averaging. As a result of these two steps, the reflectance of a few elevation zones or months is missing for several glaciers. To fill these gaps, reflectance in the same month but from different years is averaged to obtain the monthly reflectance–elevation relationships. Finally, monthly reflectance gradients for each glacier are estimated with the linear fitting method.

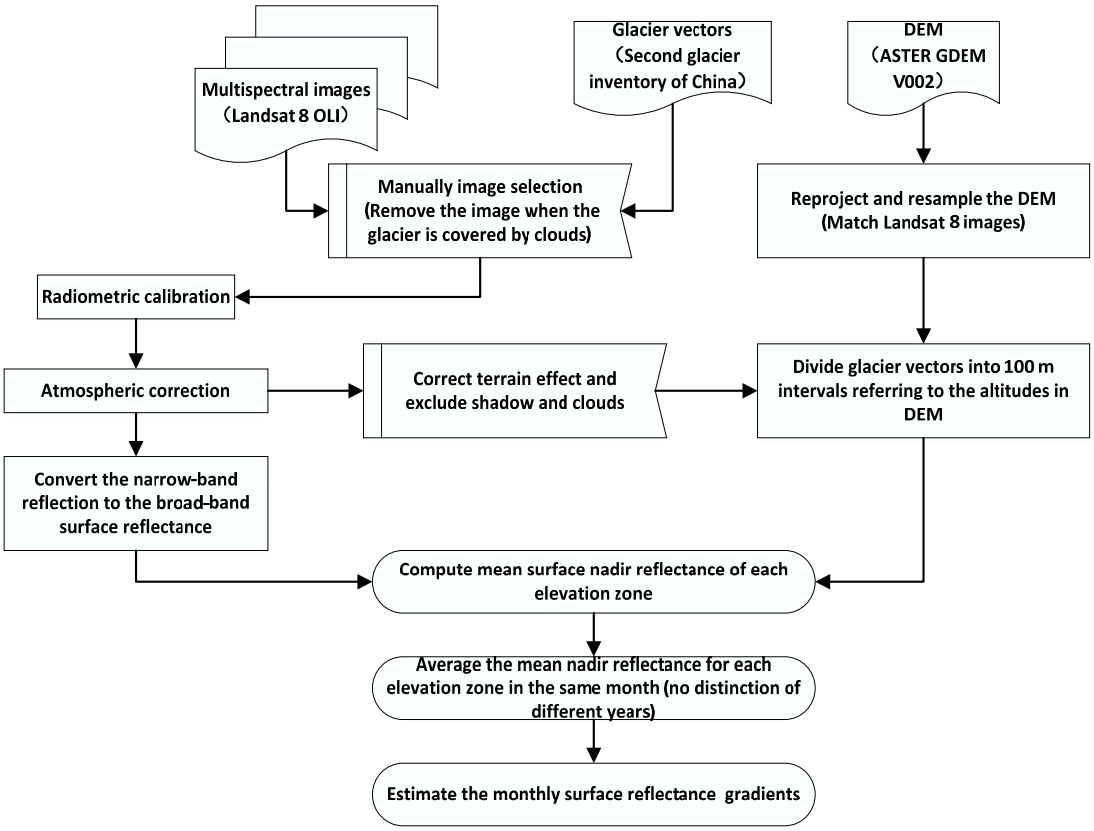

Figure 2. Workflow of monthly broadband reflectance gradient inversion.

3. Results

Examples of the extracted monthly reflectance for four glaciers are shown in Appendix A. The uncertainty is about ±0.02 [33,35]. Figures A1 and A2 show two summer accumulation type glaciers, (10) Meikuang and (12) Qiyi. For the variation of reflectance, we can see that the precipitation season is from April to October. However, in summer, because the influence of melting, the reflectance drops. Figure A3 shows the reflectance for (6) Langariding, which is a typical glacier that is affected by the Indian monsoon. Different from the former type, its reflectance is high in the cooler half-year. Figure A4 shows the results for (11) Qiumianleketage. This glacier shows relatively high reflectance all the year-round, which is a very interesting one to study. In addition, we can observe that the reflectance can vary significantly over a single glacier.

Figure 3 shows the monthly reflectance–elevation signatures for the twelve selected glaciers, with blue lines denoting winter, green lines denoting spring, red lines denoting summer, and yellow lines denoting autumn. The altitude extent used to generate the reflectance is shown in the last column of Table 1. By comparing with the original altitude extent we can see that several altitude zonesare missing in the preprocessing because of shadow, clouds, and insufficient pixels. Because mountaintops contain fewer pixels and thus are easy to be totally removed during the processing, the missing zones mainly locate in such areas. It is shown that the glacier reflectance generally increases with increasing elevation, except for the uppermost height zones of a few glaciers where the glacier flattens out and delays the downwards drainage of meltwater [4]. The detailed relationships vary between different glaciers, seasons, and altitudes. Most of the glaciers exhibit high reflectance in spring and autumn, and low reflectance in winter. This signifies spring and autumn precipitation, and dry season in winter. The climate around glaciers (1) Muji and (4) Kunjirap is especially dry, indicated by their year-round overall low reflectance. In summer, variation of reflectance gradients present an increasing trend,

especially in August for (3) Muztagata, which could be the result of the concurrent precipitation and melting in a very typical westerly region that receives rain and heat over the same period.

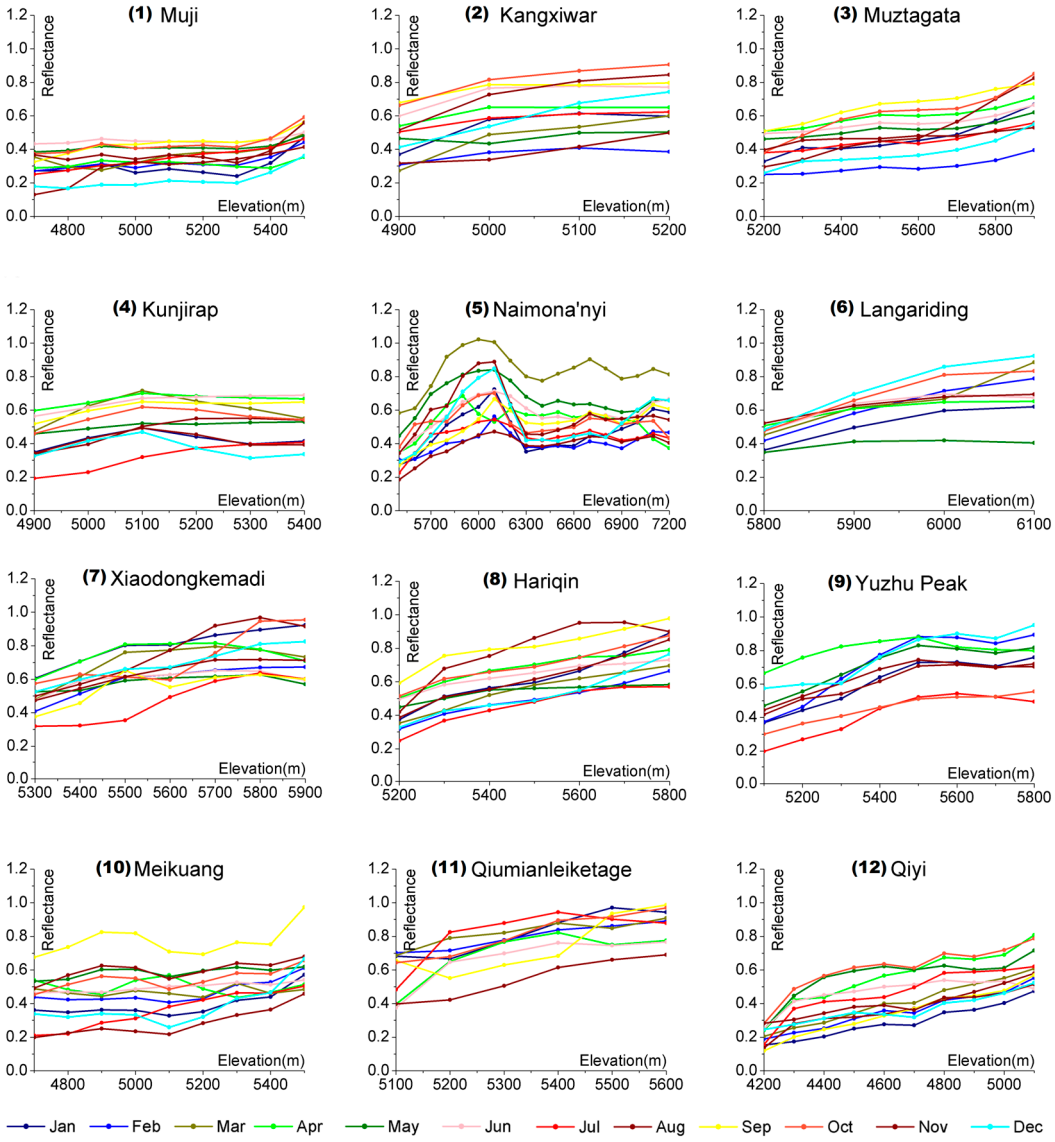

Figure 3. Monthly reflectance–elevation signatures for the twelve selected glaciers.

By observing the reflectance–elevation relationship for each glacier, several strong features can be found. (5) Naimona'nyi shows high reflectance in March, perhaps because it is in the typical Indian monsoon region with precipitation in early spring. (6) Langariding presents relatively high reflectance in winter, probably because it locates at the lowest latitude, and experiences the longest melting period. (10) Meikuang exhibits very high reflectance in September when the melt season ends in the North and precipitation remains in the central region that affected by the mixed and complex influence of westerly and Indian monsoon. Furthermore, we can observe that in both Group (A) and Group (B) selected in Section 2, glaciers with the same elevation extent show more consistent seasonal reflectance patterns than glaciers with similar locations. Therefore the reflectance–elevation relationship may dominate the seasonal reflectance variations of glaciers.

Figure 4a shows the reflectance–elevation relationship in each month for the average of twelve selected glaciers. We see a linear growing trend of the reflectance with increasing elevation, especially in the elevation range 4700–6100 m. It should be noted that after all the processing steps, only one

glacier has data when the altitude is below 4700 m ((12) Qiyi) or above 6200 m ((5) Naimona'nyi), which explains the saltation of the curve at 4700 and 6200 m. We also find that the reflectance above 6400 m is basically horizontal, which shows a stable region on the glacier where snow rarely melts. Moreover, when the altitude is over 6100 m, the reflectance declines a little because of the existence of bare rocks [36]. To eliminate the climate effect, we also present the monthly reflectance–elevation relationships using a normalized elevation in Figure 4b. Its values are obtained by denoting the reflectance variability as a ±difference to the midpoint elevation for each glacier. The mid-point elevation often serves as a proxy for the balanced budget equilibrium line altitude (ELA) [37], and thus this figure is mainly in the respect of glacier mass balance. It is shown that for most of the months, there is an obvious increasing trend of the reflectance from the lowest elevation to around +100 m. In August, the trend can hold onto +200 m because of the most severe melting in a year.

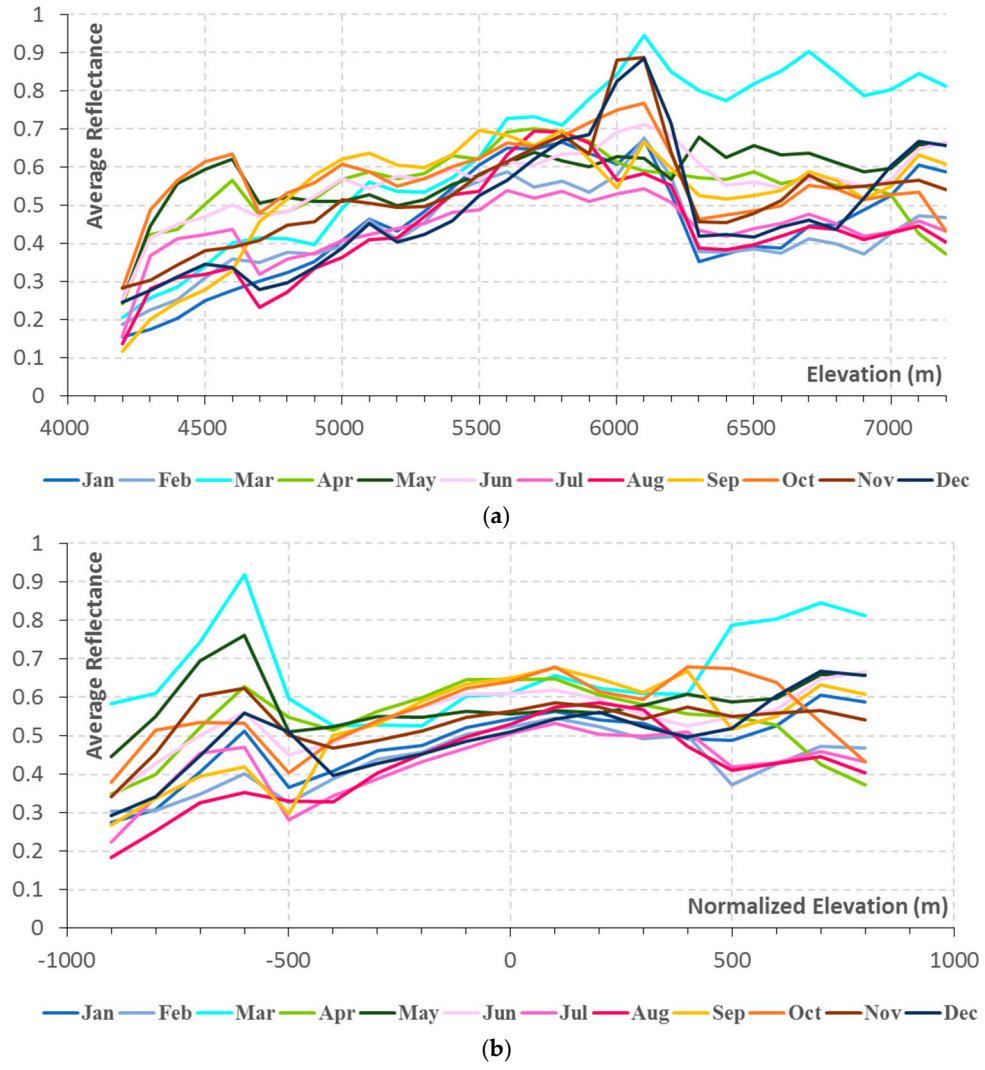

Figure 4. Monthly glacier reflectance–elevation relationship using: (**a**) the absolute elevation; and (**b**) the normalized elevation.

Table 2 shows the reflectance gradients with the blue-white-red shading denoting the low-high value. The seasonal patterns of the reflectance gradient for each glacier are shown in Figure 5. It is shown that (1) Muji, (3) Muztagata, (4) Kunjirap, (12) Qiyi and (10) Meikuang have low reflectance gradients. As mentioned above, they are glaciers in dry climate, which are in the northwest part of the Qinghai–Tibetan Plateau and are less affected by the Indian monsoon. (6) Langariding has the

highest reflectance gradients, especially in winter and early spring. This glacier receives much annual precipitation [38], and its temperature is relatively high considering its geographic location, melting in the lower parts of this glacier takes also place in winter. We can see a similar but weaker trend for (5) Naimona'nyi. We can infer from this that the overall level of glacier reflectance gradient may relate with its climate. Furthermore, from the season in which the reflectance gradient peaked, the twelve glaciers can be categorized into three classes. The first class, whose reflectance gradient peaks appear in spring and winter, includes (2) Kangxiwar, (5) Namona'nyi, (6) Langariding, and (9) Yuzhu Peak. The second class, whose reflectance gradient peaks appear in summer, includes (1) Muji, (3) Muztagata, (4) Kunjirap, (8) Hariqin, (7) Xiaodongkemadi, (10) Meikuang, and (12) Qiyi. Analyzed from the locations of these glaciers and Figure 3, we can see that the peaks of this class are mainly caused by the melting in the lower parts in summer. These peaks are not as high as those of the first type, which means that the peaks in the first type may relate with other mechanisms. There is also an atypical type which only includes (11) Qiumianleketage, whose reflectance gradient do not change much throughout the year. However, different types of glaciers seem to appear in various locations and altitudes. The surprising part is that the adjacent glaciers (9) Yuzhu and (10) Meikuang in Group (A) belong to different classes. The same situation also occurs for (2) Kangxiwa and (3) Muztagata in Group (B). However, glacier pairs with the same elevation extent in both Groups (A) and (B) are in the second class. More studies are required to understand these phenomena.

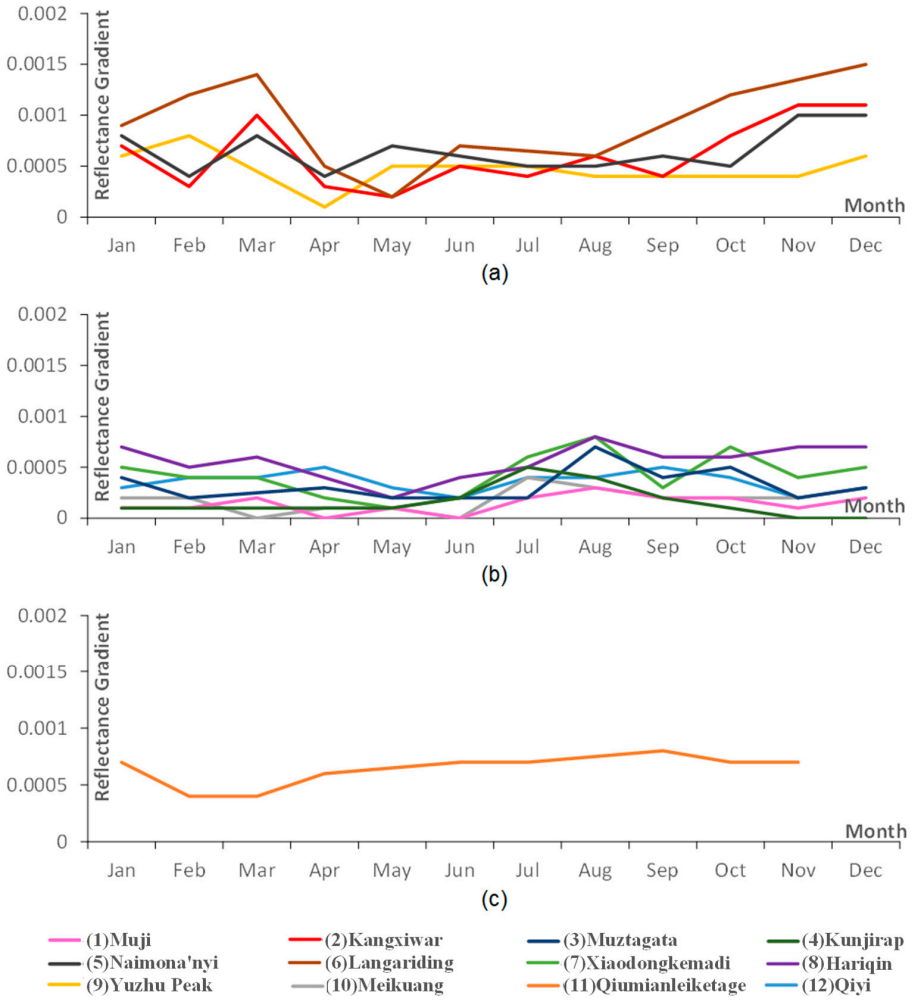

Figure 5. Seasonal patterns of glacier reflectance gradients in: (**a**) 1st class; (**b**) 2nd class; and (**c**) Qiumianleiketage.

Table 2. The reflectance gradients of linear fitting of the monthly reflectance–elevation signatures. The blue-white-red shading denotes the low-high value of reflectance gradient.

Glacier No.	1	2	3	4	5	6	7	8	9	10	11	12
January	0.0001	0.0007	0.0004	0.0001	0.0008	0.0009	0.0005	0.0007	0.0006	0.0002	0.0007	0.0003
February	0.0001	0.0003	0.0002		0.0004	0.0012	0.0004	0.0005	0.0008	0.0002	0.0004	0.0004
March	0.0002	0.001		0.0001	0.0008	0.0014	0.0004	0.0006		0	0.0004	0.0004
April	0	0.0003	0.0003	0.0001	0.0004	0.0005	0.0002	0.0004	0.0001	0.0001	0.0006	0.0005
May	0.0001	0.0002	0.0002	0.0001	0.0007	0.0002	0.0001	0.0002	0.0005	0.0001		0.0003
June	0	0.0005	0.0002	0.0002	0.0006	0.0007	0.0002	0.0004		0	0.0007	0.0002
July	0.0002	0.0004	0.0002	0.0005	0.0005		0.0006	0.0005	0.0005	0.0004	0.0007	0.0004
August	0.0003	0.0006	0.0007	0.0004	0.0005	0.0006	0.0008	0.0008	0.0004	0.0003		0.0004
September	0.0002	0.0004	0.0004	0.0002	0.0006		0.0003	0.0006		0.0002	0.0008	0.0005
October	0.0002	0.0008	0.0005	0.0001	0.0005	0.0012	0.0007	0.0006	0.0004	0.0002	0.0007	0.0004
November	0.0001	0.0011	0.0002	0	0.001		0.0004	0.0007	0.0004	0.0002	0.0007	0.0002
December	0.0002	0.0011	0.0003	0	0.001	0.0015	0.0005	0.0007	0.0006	0.0003		0.0003

4. Discussion

As far as we know, due to the limitation of the traditional earth observation systems, this is the first work that uses remote-sensing data to analyze monthly reflectance–elevation patterns. Conventional analysis usually considers variations of average albedo/reflectance of a glacier such as in [36,39,40], which is severely limited because as shown in Figure 3, the reflectance can vary significantly over a single glacier. Moreover, the reflectance is also highly related with the glacier altitude, and therefore when analyzing different glaciers, their altitude ranges should be considered. Studies in [16,20,21] take elevation into consideration. However, they only focus on a single glacier with a small altitude range, and the temporal series are also discontinuous to reveal seasonal patterns. In contrast, we present the monthly reflectance variations for twelve glaciers spanning 3100 m elevation extent which enables us to have a more comprehensive analysis.

It is interesting to see that there are peaks with reflectance around 0.9 in March, November, and December at 6100 m in Figure 4a, whereas only a March peak of 0.9 at −600 m is shown in Figure 4b. This is because some of these glaciers are in very high altitudes, which can be a special condition caused by the world's highest plateau—Tibetan Plateau. For example, when using the normalized elevation, 6100 m is only −300 m for (5) Naimona'nyi. During the averaging, the high reflectance can be easily buried with low reflectance in the same normalized elevation zone of other glaciers. The peak at −600 m is caused by the high reflectance of (5) Naimona'nyi in March. Because this elevation only exists for Naimona'nyi, the peak is kept. In Figures 6 and 7, we present the monthly reflectance–elevation relationship within 4700–6200 m (elevation zones that contain at least two chosen glaciers) using the absolute elevation, and the one obtained with the normalized elevation within ±500 m (the other elevation zones are only included for Naimona'nyi). The gradients of averaged reflectance–elevation relationships are also displayed for each month. By comparing these two figures, we can observe that glaciers with higher average elevation generally have higher reflectance which indicates that reflectance is somehow dependent on the absolute elevation, which is probably related with the special condition that the terrain in the South is higher than that in the North in western China. By considering the absolute altitude when comparing reflectance of different glaciers, it is interesting to see that in February, although the average reflectance of (5) Naimona'nyi and (12) Qiyi are similar, the relative reflectance of (12) Qiyi is higher compared to glaciers with the same altitude range, which for (5) Naimona'yi is lower. (9) Yuzhu peak commonly has higher relative reflectance than (10) Meikuang, except in November, although they are adjacent to each other. Reflectance–elevation curves are relatively separated in January whereas concentrated in June in Figures 6 and 7, which shows that the significance of climate difference varies with months. In Figure 6, the overall reflectance gradient peaks in March, while Figure 7 shows relative high reflectance gradients from June to September which corresponds to the melt season. This shows that the reflectance gradient in Figure 6 relate with the climate variation around different glaciers. In Figure 7, we can see that the abruption point of the

melting region for (5) Naimona'yi is extremely low (around −300 m), which indicates that using the midpoint elevation to approximate the ELA maybe not suitable for glaciers with such a high altitude. Those analyses demonstrate that with the extracted reflectance of each 100 m altitude zone in each month, more interesting information can be observed and we can have a better understanding of the spatial and temporal variations of glacier reflectance.

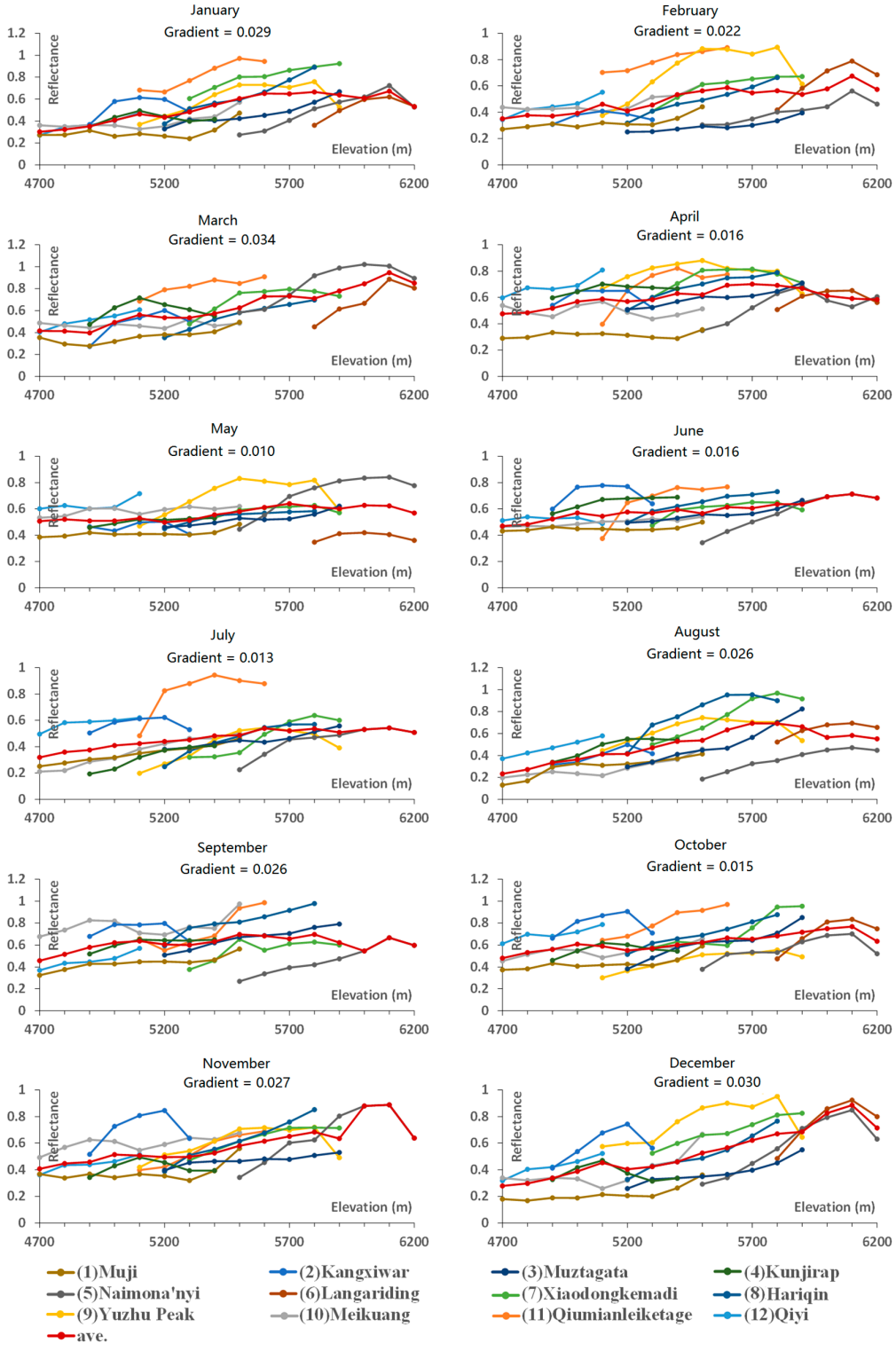

Figure 6. Monthly reflectance–elevation relationship for each glacier using absolute elevation. The gradient presented in each month is obtained using the average reflectance.

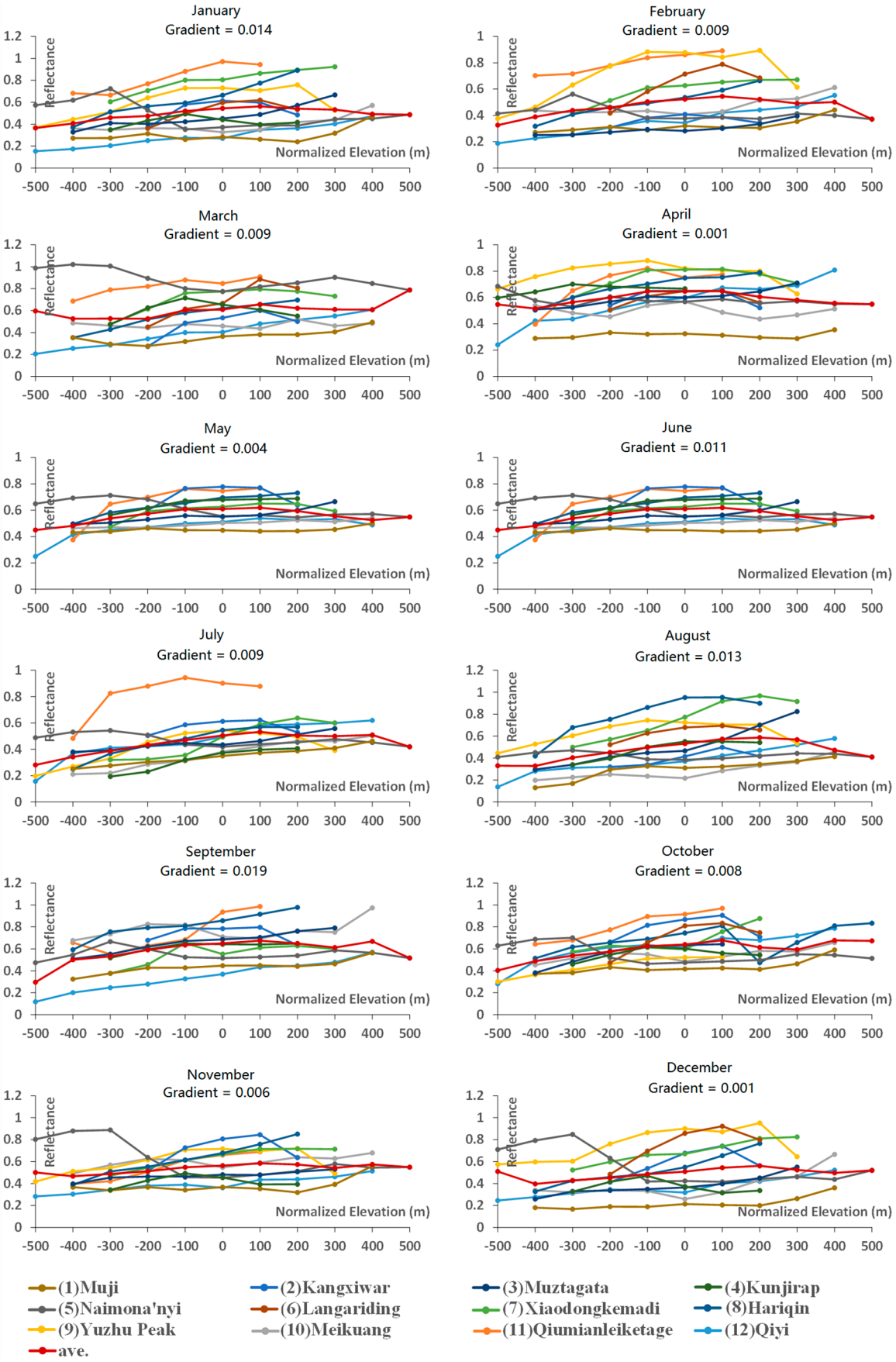

Figure 7. Monthly reflectance–elevation relationship for each glacier using normalized elevation. The gradient presented in each month is obtained using the average reflectance.

To examine the linear trend of glacier reflectance–elevation relationships, we calculate the R^2 of the linear fitting when $p < 0.05$ for each glacier and each month. The cases of $R^2 < 0.5$ only account for 13% of the total amount and correspond to very low gradients. Except for these situations, the overall goodness of fit is very high. Moreover, the R^2 for the linear fitting of the average reflectance–elevation curves shown in Figure 4a are also high (>0.65 in eleven months and 0.42 in May), which proves the linear trend of the general reflectance–elevation relationship for glaciers. Using median instead of average could be more robust to further reduce the impact of outliers, which we will attempt in future work. The averaging of pixels within the same elevation zone enhances the robustness of the estimation. It should be noted that even with the acquisition ability of Landsat 8, the time series of a glacier in one year is mostly fragmentary. Every year will have several months missing because of cloud cover. Although a few measures have been taken, we have not found a better way to completely solve this problem. In addition, we think presenting a fragmentary time series for only one particular year may be not representative. Therefore, in each month, we use the average reflectance of three years (when at least two images are acquired during 2013–2015). This may include bias because of the likely high variability of snow cover from year to year, but if the snowfall did happen in one year, it could happen in another year. We will not know for sure in which year the weather is more representative, and we believe that the climate will not change significantly in three years. Therefore, we think this is so far the closest study to acquire the monthly pattern of glacier reflectance–elevation relationships.

5. Conclusions

We have obtained the monthly variations of reflectance and reflectance gradients for twelve glaciers in western China based on 372 Landsat 8 images collected from April 2013 to December 2015. From our results, we draw the following conclusions. Reflectance generally shows a raising trend with increasing elevation (when the altitude is less than 6100 m). The overall goodness of fit of the linear fitting is very high, which proves the linear trend of the reflectance–elevation relationship, though the detailed relationships vary between different glaciers, seasons and altitudes. Glaciers with the same elevation extent show seasonal reflectance patterns of higher consistency than glaciers with similar location, which means the reflectance–elevation relationship dominates the seasonal variations of glacier reflectance. Therefore, when comparing different glaciers, their absolute altitude ranges should be considered. Glaciers in north and dry climate such as (1) Muji, (3) Muztagata, (4) Kunjirap, (10) Meikuang, and (12) Qiyi show low reflectance gradients. Glaciers in south and wet climate such as (5) Naimona'nyi and (6) Langariding show high reflectance gradients, especially in winter and spring. This indicates that the overall level of glacier reflectance gradient may relate with its climate. The twelve glaciers can be categorized into three classes according to the seasons in which the signature of reflectance gradients peaked: (i) reflectance gradient peaks in spring and winter; (ii) reflectance gradient peaks in summer; and (iii) reflectance gradients show no significant change throughout the year. However, different types of glaciers seem to appear at various locations and altitudes. Further effort is needed to understand these classes.

Acknowledgments: This work was funded by the key laboratory of Tibetan environment changes and land surface processes, Chinese Academy of Sciences, and the 13th Five Year Plan Project of the Chinese Academy of Sciences (Grant No. Y6SG0400CX).

Author Contributions: Xinwu Li and Baiqing Xu conceived and designed the experiments; Siyang Yin, Ruifang Yang, and Shu Cheng performed the experiments; and Wenjin Wu analyzed the data and wrote the paper.

Conflicts of Interest: The authors declare no conflict of interest. The founding sponsors had no role in the design of the study; in the collection, analyses, or interpretation of data; in the writing of the manuscript, and in the decision to publish the results.

Appendix

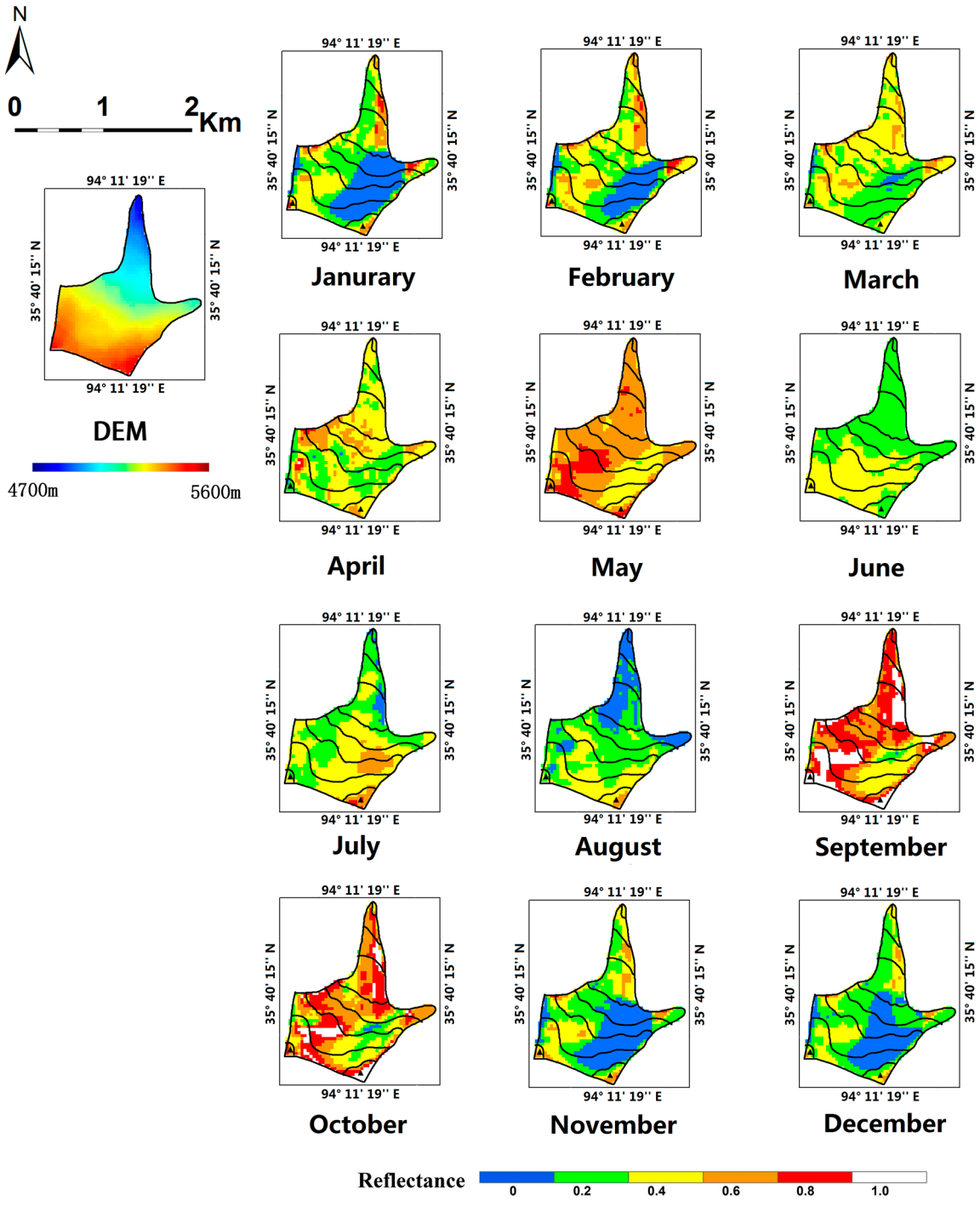

Figure A1. Monthly glacier reflectance of (10) Meikuang.

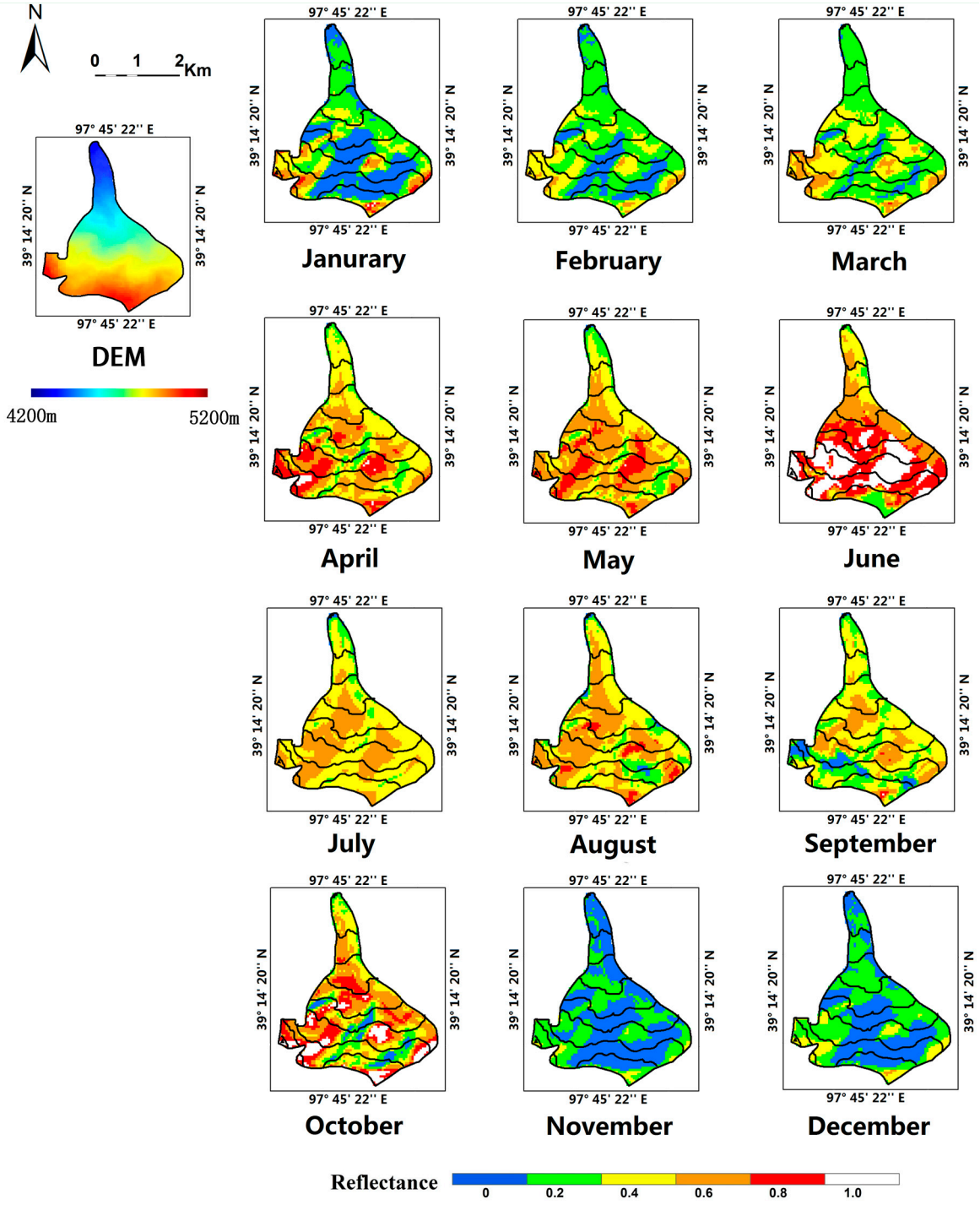

Figure A2. Monthly glacier reflectance of (12) Qiyi.

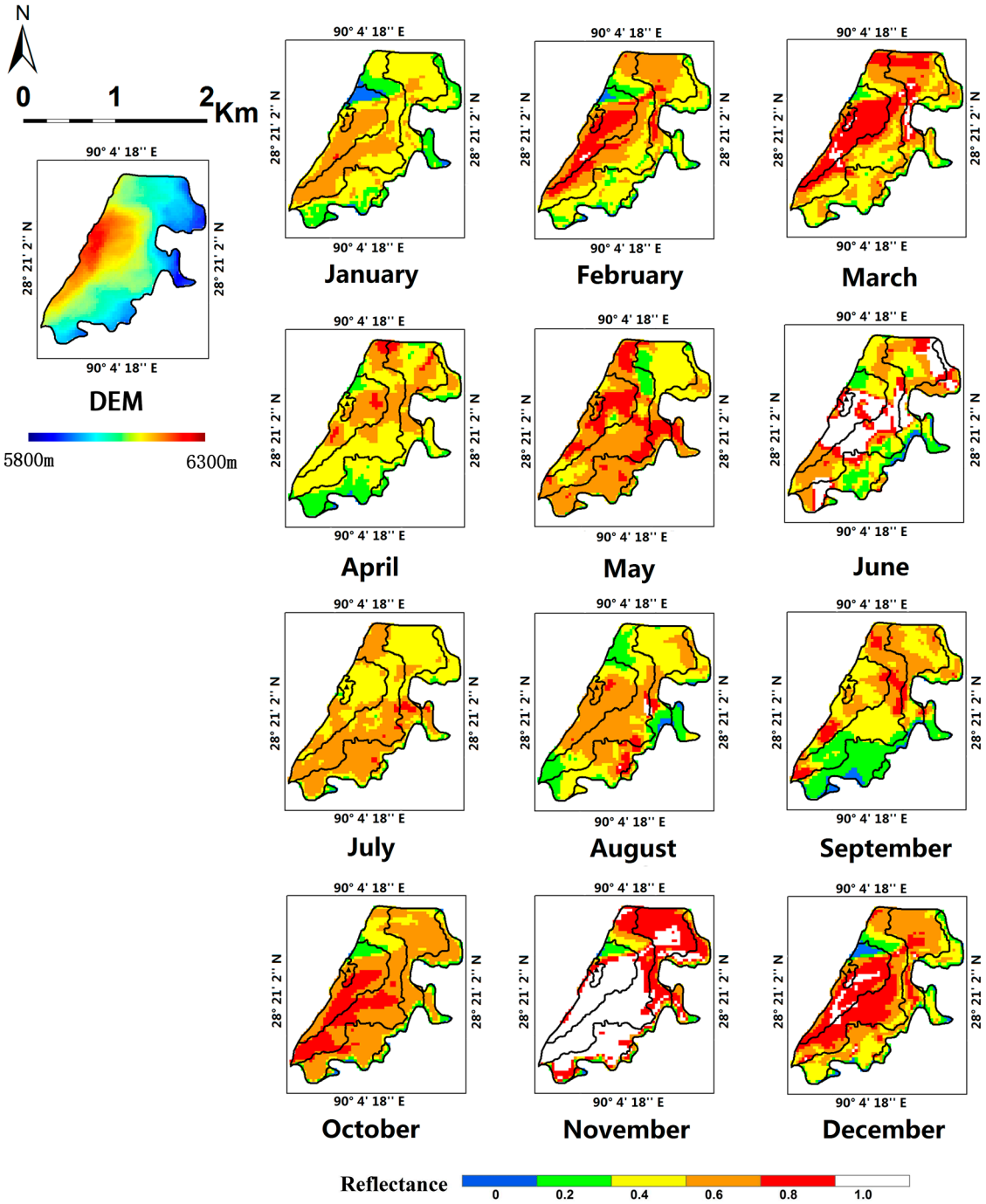

Figure A3. Monthly glacier reflectance of (6) Langariding. Results in July, September, and November are excluded in the post-processing due to insufficient image quality (e.g., affected by thin cloud and fog).

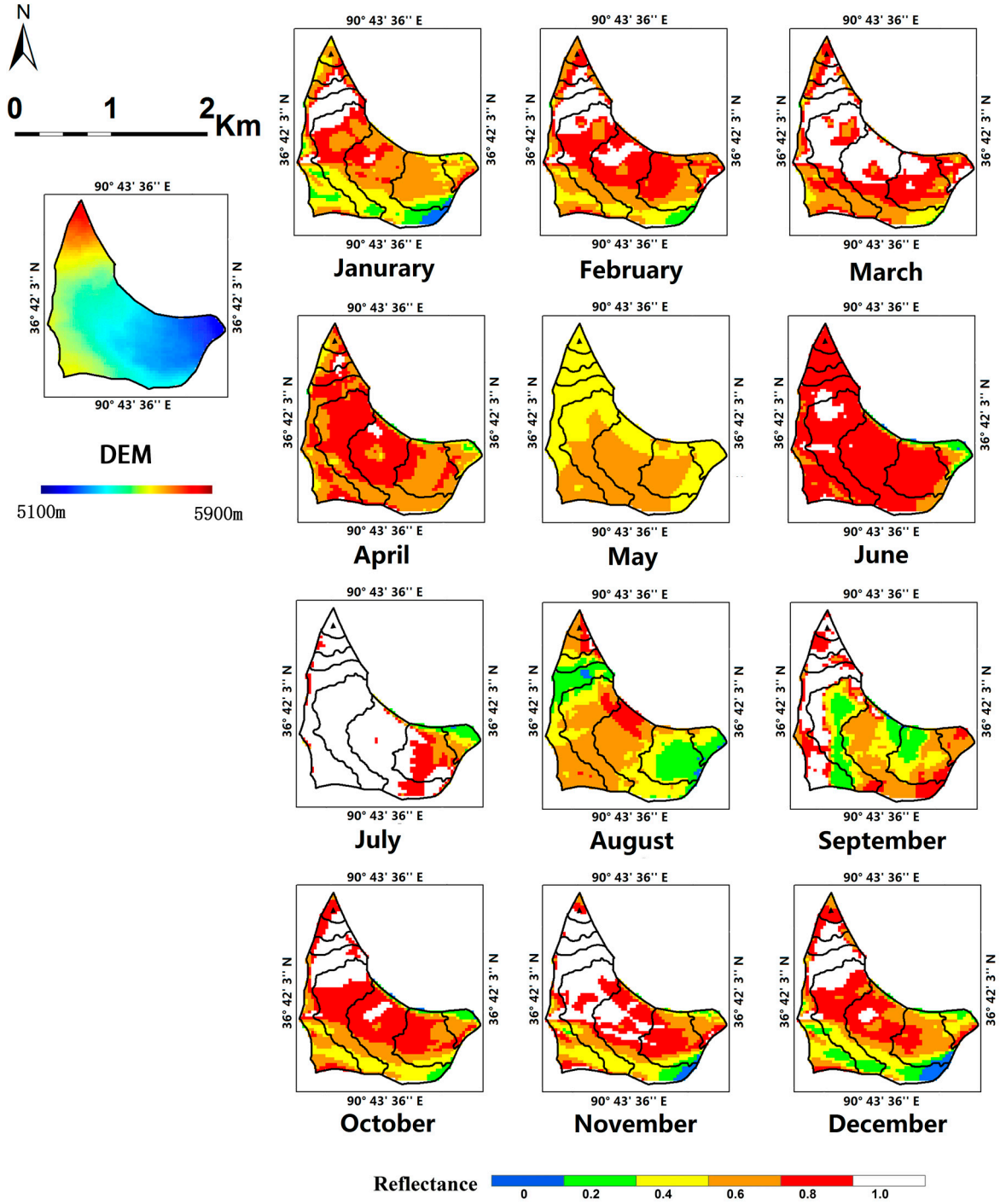

Figure A4. Monthly glacier reflectance of (11) Qiumianleiketage. Results in May and August are excluded in the post-processing due to insufficient image quality (e.g., affected by thin cloud and fog).

References

1. Zhang, Y.; Yao, T.; Pu, J.; Ohata, T.; Yabuki, H.; Fujita, K. Energy budget at ELA on Dongkemadi Glacier in the Tonggula Mts. Tibetan Plateau. *J. Glaciol. Geocryol.* **1996**, *18*, 10–19.
2. Takeuchi, N. Temporal and spatial variations in spectral reflectance and characteristics of surface dust on Gulkana Glacier, Alaska Range. *J. Glaciol.* **2009**, *55*, 701–709. [CrossRef]
3. Lhermitte, S.; Abermann, J.; Kinnard, C. Albedo over rough snow and ice surfaces. *Cryosphere* **2014**, *8*, 1069–1086. [CrossRef]

4. Winther, J.G. Landsat TM derived and in situ summer reflectance of glaciers in Svalbard. *Polar Res.* **1993**, *12*, 37–55. [CrossRef]
5. Reijmer, C.H.; Knap, W.H.; Oerlemans, J. The surface albedo of the Vatnajökull ice cap, Iceland: A comparison between satellite-derived and ground-based measurements. *Bound. Layer Meteorol.* **1999**, *92*, 123–143. [CrossRef]
6. Pirazzini, R. Surface albedo measurements over Antarctic sites in summer. *J. Geophys. Res. Atmos.* **2004**, *109*. [CrossRef]
7. Stroeve, J.; Box, J.E.; Gao, F.; Liang, S.; Nolin, A.; Schaaf, C. Accuracy assessment of the MODIS 16-day albedo product for snow: Comparisons with Greenland in situ measurements. *Remote Sens. Environ.* **2005**, *94*, 46–60. [CrossRef]
8. Stroeve, J.C.; Box, J.E.; Haran, T. Evaluation of the MODIS (MOD10A1) daily snow albedo product over the Greenland ice sheet. *Remote Sens. Environ.* **2006**, *105*, 155–171. [CrossRef]
9. Dumont, M.; Sirguey, P.; Arnaud, Y.; Six, D. Monitoring spatial and temporal variations of surface albedo on Saint Sorlin Glacier (French Alps) using terrestrial photography. *Cryosphere* **2011**, *5*, 759–771. [CrossRef]
10. Dumont, M.; Gardelle, J.; Sirguey, P.; Guillot, A.; Six, D.; Rabatel, A.; Arnaud, Y. Linking glacier annual mass balance and glacier albedo retrieved from MODIS data. *Cryosphere* **2012**, *6*, 1527–1539. [CrossRef]
11. Pope, E.L.; Willis, I.C.; Pope, A.; Miles, E.S.; Arnold, N.S.; Rees, W.G. Contrasting snow and ice albedos derived from MODIS, Landsat ETM+ and airborne data from Langjökull, Iceland. *Remote Sens. Environ.* **2016**, *175*, 183–195. [CrossRef]
12. Schaaf, C.; Wang, Z. MCD43D16: MODIS/Terra+Aqua BRDF/Reflectance Parameter1 Band6 Daily L3 Global 30ArcSec CMG V006. NASA EOSDIS Land Processes DAAC. Available online: http://doi.org/10.5067/MODIS/MCD43D16.006 (accessed on 1 January 2015).
13. Kovalskyy, V.; Roy, D.P. The global availability of Landsat 5 TM and Landsat 7 ETM+ land surface observations and implications for global 30 m Landsat data product generation. *Remote Sens. Environ.* **2013**, *130*, 280–293. [CrossRef]
14. Roy, D.P.; Wulder, M.A.; Loveland, T.R.; Woodcock, C.E.; Allen, R.G.; Anderson, M.C.; Helder, D.; Irons, J.R.; Johnson, D.M.; Kennedy, R.; et al. Landsat-8: Science and product vision for terrestrial global change research. *Remote Sens. Environ.* **2014**, *145*, 154–172. [CrossRef]
15. Penitente (Snow Formation). Available online: https://en.wikipedia.org/wiki/Penitente_(snow_formation) (accessed on 6 January 2017).
16. Jonsell, U.; Hock, R.; Holmgren, B. Spatial and temporal variations in albedo on Storglaciären, Sweden. *J. Glaciol.* **2003**, *49*, 59–68. [CrossRef]
17. Takeuchi, N.; Uetake, J.; Fujia, K.; Aizen, V.B.; Nikitin, S.D. A snow algal community on Akkem glacier in the Russian Altai mountains. *Ann. Glaciol.* **2006**, *43*, 378–384. [CrossRef]
18. Wang, J.; Cui, Y.; He, X.; Zhang, J.; Yan, S. Surface Reflectance Variation and Its Influencing Factors over Dongkemadi Glacier, Central Tibetan Plateau. *Adv. Meteorol.* **2015**, *2015*, 10–13. [CrossRef]
19. Takeuchi, N.; Koshima, S.; Segawa, T. Effect of cryoconite and snow algal communities on surface albedo on maritime glaciers in south Alaska. *Bull. Glaciol. Res.* **2003**, *20*, 21–27.
20. Takeuchi, N. Seasonal and altitudinal variations in snow algal communities on an Alaskan glacier (Gulkana glacier in the Alaska range). *Environ. Res. Lett.* **2013**, *8*, 035002. [CrossRef]
21. Brock, W.; Willis, C.; Sharp, J. Measurement and parameterization of albedo variations at Haut glacier d'Arolla, Switzerland. *J. Glaciol.* **2000**, *46*, 675–688. [CrossRef]
22. Landsat Science. Available online: http://landsat.gsfc.nasa.gov/landsat-8/landsat-8-overview/ (accessed on 6 January 2017).
23. Fujita, K. Effect of precipitation seasonality on climatic sensitivity of glacier mass balance. *Earth Planet. Sci. Lett.* **2008**, *276*, 14–19. [CrossRef]
24. Naito, N.; Nakawo, M.; Kadota, T.; Raymond, C.F. Numerical simulation of recent shrinkage of Khumbu Glacier, Nepal Himalayas. In *Debris-Covered Glaciers: Proceedings of an International Workshop Held at the University of Washington, Seattle, WA, USA, 13–15 September 2000*; International Association of Hydrological Sciences: Wallingford, UK, 2000.
25. ArcGIS Blog: Hill Shade. Available online: https://blogs.esri.com/esri/arcgis/2014/07/14/introducing-esris-next-generation-hillshade/ (accessed on 6 January 2017).

26. The Second Glacier Inventory of China. Available online: http://westdc.westgis.ac.cn/data/f92a4346-a33f-497d-9470--2b357ccb4246 (accessed on 6 January 2017).
27. NASA LP DAAC. *ASTER Global Digital Elevation Model V002*; NASA EOSDIS Land Processes DAAC; USGS Earth Resources Observation and Science (EROS) Center: Sioux Falls, SD, USA, 2015.
28. Warp and Resample. Available online: http://www.harrisgeospatial.com/docs/WarpingResampling.html (accessed on 6 January 2017).
29. Using the USGS Landsat 8 Product. Available online: https://landsat.usgs.gov/using-usgs-landsat-8-product (accessed on 28 January 2017).
30. Bernstein, L.S.; Adler-Golden, S.M.; Sundberg, R.L.; Levine, R.Y.; Perkins, T.C.; Berk, A.; Ratkowski, A.J.; Felde, G.; Hoke, M.L. Validation of the QUick Atmospheric Correction (QUAC) algorithm for VNIR-SWIR multi- and hyperspectral imagery. *Proc. SPIE* **2005**, *5806*, 668–678.
31. Berk, A.; Bernstein, L.S.; Anderson, G.P.; Acharya, P.K.; Robertson, D.C.; Chetwynd, J.H.; Adler-Golden, S.M. MODTRAN Cloud and Multiple Scattering Upgrades with Application to AVIRIS. *Remote Sens. Environ.* **1998**, *65*, 367–375. [CrossRef]
32. Bernstein, L.S.; Jin, X.; Gregor, B.; Adler-Golden, S.M. Quick atmospheric correction code: Algorithm description and recent upgrades. *Opt. Eng.* **2012**, *51*, 111719. [CrossRef]
33. Liang, S.L. Narrowband to broadband conversions of land surface albedo I: Algorithms. *Remote Sens. Environ.* **2001**, *76*, 213–238. [CrossRef]
34. Mort Canty's Software. Available online: http://mortcanty.github.io/src/software.html (accessed on 3 April 2016).
35. Liang, S.L.; Shuey, C.J.; Russ, A.L.; Fang, H.; Chen, M.; Walthall, C.L.; Daughtry, C.S.T.; Hunt, R., Jr. Narrowband to broadband conversions of land surface albedo II: Validation. *Remote Sens. Environ.* **2002**, *84*, 25–41. [CrossRef]
36. Mao, R.; Wu, H.; He, J. Spatiotemporal variation of albedo of Muztagh Glacier in the Kunlun Mountains and its relation to dust. *J. Glaciol. Geocryol.* **2013**, *35*, 1133–1142.
37. Braithwaite, R.J.; Raper, S.C.B. Estimating equilibrium-line altitude (ELA) from glacier inventory data. *Ann. Glaciol.* **2009**, *53*, 127–132. [CrossRef]
38. China Climate Map-Precipitation. Available online: http://www.chinamaps.org/china/china-map-of-precipitation.html (accessed on 28 January 2017).
39. Brun, F. Seasonal changes in surface albedo of Himalayan glaciers from MODIS data and links with annual mass balance. *Cryosphere* **2015**, *9*, 341–355. [CrossRef]
40. Jakob, A.; Christophe, K.; Shelley, M. Albedo variations and the impact of clouds on glaciers in the Chilean semi-arid Andes. *J. Glaciol.* **2014**, *60*, 183–191.